Design of a SI Cuk Converter based on Bridgeless Power Factor Correction with Regenerative Braking

Swaliyabegum Mulla[1][a] and M. S. Aspalli[1][b]

Department of Electrical and Electronics Engineering (Affiliated to VTU Belgaum)
Poojya Doddappa Appa College of Engineering, Kalaburagi (Affiliated to VTU Belgaum), Karnataka, India

Keywords: Cuk Converter, Power Factor Correction, High Gain Converter, Regenerative Braking.

Abstract: The size of a switched inductor (SI) based Cuk converter is lowered with increased power factor when the bridge is removed from an electric car charging system. The traditional techniques for battery charging involve two-stage power conversion. The single stage switching inductor topology improves the voltage conversion ratio. A high gain bidirectional converter is introduced to power the motor for the operation of an electric vehicle after the performance of the converter under steady state and transient situations is noted. Software called MATLAB/Simulink is used to carry out the simulation job. In order to verify that the suggested system operates as intended, a hardware model is created.

1 INTRODUCTION

Given the constantly increasing share of demand for LEVs, the charging station outfitted utilizing a superior method for improving power quality is highly anticipated from the perspectives of both power distributors and users. The current generation of LEV chargers frequently begin with a dc-dc converter that is either isolated or not, together with a configuration of an unregulated rectifier and a dc bus capacitor. When DBR and a big dc-link capacitor are used together, the input's power factor (PF) and overall system efficiency all suffer because they draw harmonics-rich distorted current from the supply. Power factor correction (PFC) largely eliminates these flaws in conventional low power rating converters. In an APFC approach, a dc-dc converter is employed between DBR and CDC to improve the source side of the converter's performance from the standpoint of power quality(Lachvajderova et al,2021)(Wang et al,2021). It is crucial to understand that an APFC conversion, whether it is a single-stage converter or a two-stage converter with differentconfigurations, can perform a variety of tasks in a charger. In a two -stage setup, an APF cuk

converter is utilized to satisfy source requirements, while a second dc-dc converter is required to satisfy load requirements. In single-stage converters, however, a single APF cuk converter fulfils both criteria. A number of two-stage converter designs based on various APFC techniques have been researched for the purpose of charging EVs and LEVs. Each technique has benefits and drawbacks in terms of component tally, conductance and switch losses, control complexity, and effectiveness. To improve efficiency by reducing conduction losses on the APF cuk conversion stage, several bridgeless APFC converters with partial or complete deletion of the DBR have been recorded in the literature. The presentation includes a full investigation of bridgeless APF cuk converters (Bahrami et al,2020). Certain bridgeless integrated charging techniques have recently been presented as a way to keep the advantages of two-stage converters while reducing the number of parts and inefficiencies in the chargers (Dulau at al.,2020). Integration of the power electronic equipment reduces the overall number of devices and associated losses. However, the rising control complexity and high device pressures account for their diminished appeal for LEV applications. The ripple-free charging current is one of the two-stage converter's primary advantages. The performance of the battery, as has been asserted by a number of authors, is unaffected by low-frequency fluctuations in the pushing current when they are properly

_____

[a] https://orcid.org/0009-0001-4998-6785
[b] https://orcid.org/0000-0002-5483-6415

regulated (Rachid et al., 2022). To address these issues with two-stage converters, numerous researchers have proposed alternate single-stage converter topologies for EVs/LEVs together with enhanced power quality at the source side. The single-stage converters provide a low component count, high power density, and an easy-to-understand control design (Habib,2018). A properly designed single-stage converter configuration may also provide superior efficiency compared to its two-stage converter. The common buck converter's high supply current distortion at the zero crossing and the standard boost converter's constrained output voltage capabilities exclude their possible usage as an APFC in single-stage LEV converters. The disadvantages of buck and boost derived converters are therefore typically eliminated when utilizing buck-boost derived converters. The Cuk model of buck-boost dc-dc converters has the least amount of output and input current ripple. Traditional buck-boost dc-dc converters, on the other hand, are less suitable to provide a transformerless single-stage conversion for the LEVs due to their low gain capabilities. Due to the low battery voltage, the transformerless charger architecture in LEVs operates at an extremely low duty ratio, which eventually affects the charger's dynamic efficiency and performance. The common buck converter's high supply current distortion at the zero crossing and the standard boost converter's constrained output voltage capabilities exclude their possible usage as an APFC in single-stage LEV converters. The disadvantages of buck and boost derived converters are therefore typically eliminated when utilizing buck-boost derived converters. The Cuk model of buck-boost dc-dc converters has the least amount of output and input current ripple. Traditional buck-boost dc-dc converters, on the other hand, are less suitable to provide a transformerless single-stage conversion for the LEVs due to their low gain capabilities. Due to the low battery voltage, the transformerless charger architecture in LEVs operates at an extremely low duty ratio, which eventually affects the charger's dynamic efficiency and performance. Therefore, the majority of single-stage LEV converters based on conventional dc-dc converters require a transformer in order to achieve the required dc voltage gain. However, the transformer drives up the cost and size of the charger. The leakage inductance of the transformer also increases the voltage stress between the parts. The transformerless charger architecture for LEVs based on improved power quality is still seldom ever discussed in academia. coupling inductors, converter cascading, the use of multipliers, interleaved front

end structures, switched inductors, and hybrid switched inductor-capacitor structures are recent developments (Khalid et,2021) (Das et al,2021). However, in the case of linked inductors, the coupling coefficient has a significant impact on the operational parameters of the converter. The quadratic converter is more effective than a cascaded converter at adjusting for increasing voltage and current stresses. As a remedy to these issues, a switching dual network composed of two to three diodes, split type inductors, or capacitors is proposed. This charger is costly, has a challenging control system, and has larger magnetic components due to the CCM operation. This research presents a single-stage Cuk converter-based modified power factor improved converter. Because the dcm mode of operation eliminates the need for sensors, the controller design is straightforward. The converter's bridgeless design results in a significant reduction in the number of components used. The proposed converter is put to the test using constant voltage and constant current control techniques with variable input voltage conditions. Once the vehicle is running on battery power, the motor is powered via a high gain bidirectional converter. Regenerative braking can be used and extend the vehicle's running time because of the bidirectional property.

2 SYSTEM DESCRIPTION

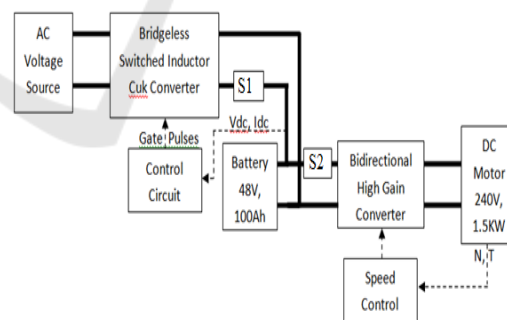The proposed system is provided below in Fig 1.

Fig 1: Proposed system Block diagram.

The ac supply is connected to the BSIC converter in this case while the car is charging so that the battery can be charged while switch 1 (S1) is ON and switch 2 (S2) is OFF. The battery serves as the load in this. The control loop regulates the voltage and current of the battery. S1 is OFF (the ac source is disconnected) and S2 is ON (the motor is connected) when the car starts. The battery serves as the supply in this. The measured speed of the DC motor is fed into the speed

control loop, which regulates the output voltage of the bidirectional converter, causing the measured speed to match the reference speed.

2.1 BSIC Converter and Control

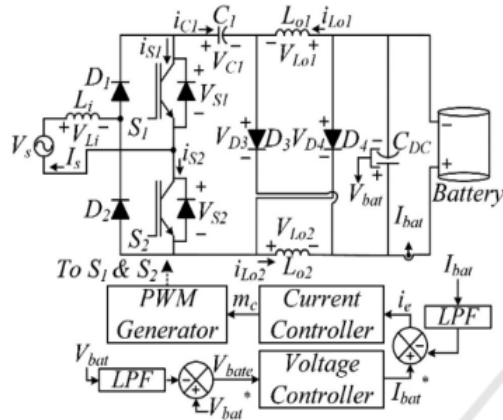The bridgeless Cuk converter circuit is provided below:

Fig 2: circuit diagram for Single phase Single.

Stage Bridgeless switched Inductor Cuk Converter (BSIC) Power Factor Correction(PFC) Converter.

This configuration offers a single-stage ac-dc converter with high voltage conversion capability and superior power quality on the supply side for the LEV charging application. The rated voltage (Vs) specification for the single-phase supply that powers the bridgeless construction on the front end is 220 V, 50 Hz. The source inductor (Li) serves as the input inductor for the Cuk converter as well as a gradient with the source current (Is). The leading leg of the rectifier bridge is made up of diodes, D1 and D2, while the second leg is made up of two active switches, S1 and S2. This differs from the standard DBR, which consists of a combination of four diodes. In order to reduce control complexity, While the switches (S1 and S2) run simultaneously regardless of the supply voltage polarity, D1 and D2 operate during each of the supply voltage's two half-cycles, respectively.

On the load side, a SI network is provided that combines two inductors (Lo1 and Lo2) with two diodes (D3 and D4). The total gain of the charger is improved by charging the output inductors in series and discharging them in parallel. A battery with a 48 V and 1.3 Ah voltage rating serves as the load. The converter control is also made simpler and less expensive by employing the fewest number of

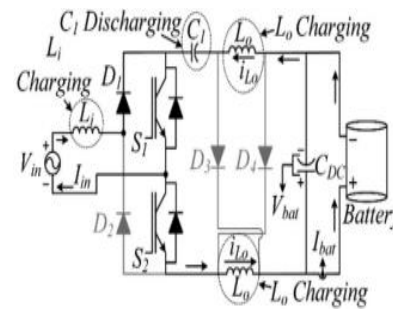sensing devices possible to implement the charger's control.

Fig 3: mode 1 operation of BSIC.

The following list includes the aforesaid converter's operational modes:

Mode 1:

In this, the source side inductance and both power electronic switches S1 and S2 are in operation. With the help of the input voltage source, Li is being charged, while C1 is being discharged to supply power to the inductors Lo and battery.

Mode 2:

In this case, the input side inductor begins to discharge while both power electronic switches are in the OFF state. Along with conducting is the body diode of S2, the diodes D1, D3, and D4. While the inductors Lo are discharging, the capacitors C1 begins to charge.
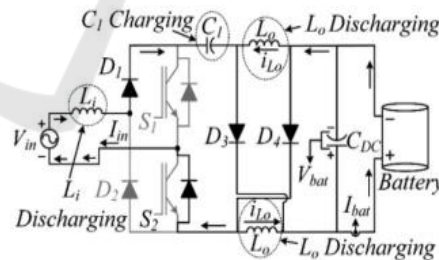

Fig 4: Operation of Mode 2 of BSIC.

Mode 3:

The diodes D3 and D4 stop conducting because of the reverse bias. While C1 is still charging, the input side inductance Li is still discharging. The inductors' Low state allows the current to freely flow through them without being charged or discharged.
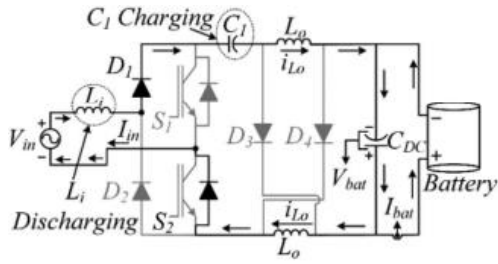
Fig 5: Operation of Mode 3 of BSIC.

The voltage conversion ratio of the cuk converter is provided below:

$$V_{bat} = V_{in} \cdot D/(2*D_1) = M \cdot V_{in}.$$

where D1 represents the diodes (D5 and D6) duty ratio and M= Vbat/Vin.

The load side inductance value is calculated as provided below:

$$L_{ocritical} = R_{L\min}/\left[f_s \cdot (1 + 2 \cdot M_{max})\right]$$

The source side inductance value is calculated for CCM is provided below:

$$C_1 = 1/\left\{\omega_{res}^2 \cdot (L_i + L_{o1} + L_{o2})\right\}$$

$$L_{icritical} = \frac{V_{inmax}^2 \cdot D_{max}}{P_{max} \cdot \chi \cdot f_s} = \frac{(\sqrt{2} \cdot V_{smax})^2 \cdot D_{max}}{P_{max} \cdot \chi \cdot f_s}$$

The value of C1 is calculated as

where ωres is resonant frequency

CDC is calculated as

$$C_{DC} = P_{max}/(4\pi \cdot f_{Line} \cdot \lambda \cdot V_{batmax}^2)$$

where f_{line} is the supply frequency.

2.2 High Gain Boost Converter

Similar to a resistor, an inductor behaves as an appliance and uses energy when it is charged, and when it is discharged, it acts as a source of energy. Because the voltage it creates during the phase of discharge is based on the rate of current change rather than the starting charging voltage, a variety of voltages at the input and output are possible. The following graphic shows the basic layout for a boost converter with a high voltage conversion ratio:
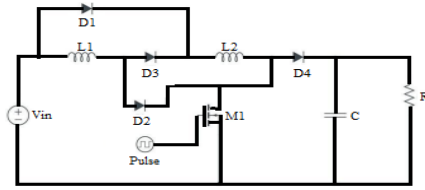

Fig 6: Basic configuration of high gain boost converter.

The proposed converter operates in one of two modes while the power electronic switch S is in operation and in both modes when switch S is turned off. Inductors L1 and L2 get charged simultaneously by the source voltage Vin through Diodes D1 and D2, respectively, when switch S is switched ON. A single capacitor, four diodes, and a MOSFET switch with a PWM switching rate make up the power circuit approach. Capacitor C is discharged by the load. D3 and D4 reverse biased diodes were available. The operation is depicted in the accompanying figure while switch S is turned ON.
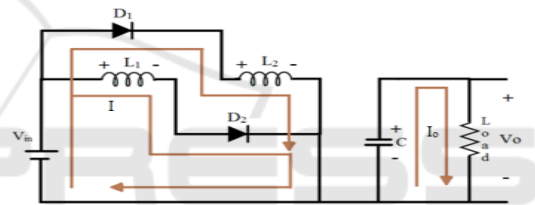

Fig 7: Operation of converter when switch is ON.

Both inductors are draining while the power electronic switch S is turned off, and the voltage source is connected in series by diodes D3 and D4. D1 and D2 are not conducting at this time.
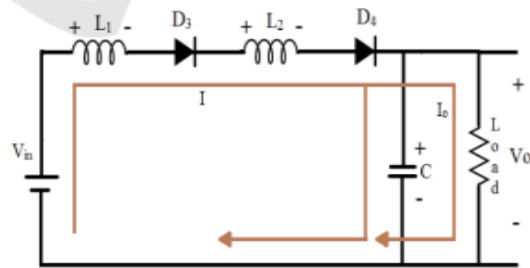

Fig 8: Operation of converter when switch is OFF.

The design equations for the high gain dc-dc converter is provided below:

The duty ratio of the high gain converter is provided below.

$$\frac{V_o}{V_{in}} = \frac{1+D}{1-D}$$

The inductor ripple current is provided below

$$\Delta I_L = (0.2 \text{ to } 0.4) \times I_{OUT(max)} \times \frac{V_{OUT}}{V_{IN}}$$

The inductor value is provided by the relation shown below

$$L = \frac{V_{IN} \times (V_{OUT} - V_{IN})}{\Delta I_L \times f_S}$$

The load capacitor value is calculated as follows:

$$C_{OUT(min)} = \frac{I_{OUT(max)} \times D}{f_S \times \Delta V_{OUT} (1-D)}$$

Where ΔV_{OUT} = desired output voltage ripple.

Switches Q2 and Q3 are used in place of the diodes D2 and D3 for bidirectional power flow; Q3 works at a PWM frequency while Q2 operates at a lower frequency solely to provide a path for the load (the battery serves as the load during regenerative braking).
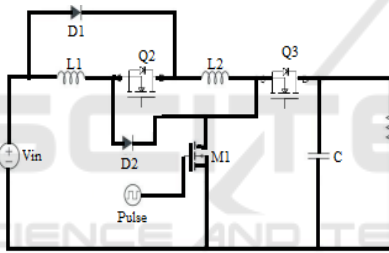

Fig 9: circuit diagram of converter when diodes are placed with switches Q1&Q2.

2.3 Control Structure of Basic Converter

The suggested converter is used to control the battery's charging current in both CC and CV modes, depending on the circumstance. While the outer loop controls variations in Vbat, the inner loop controls Ibat and maintains UPF operation with the least amount of distortion. The reference battery current (Ibat) is obtained by matching the Vbat and Vbat for the outer loop, and the error (Vbate) is fed into the proportional-integral (PI) control as an input. The voltage PI controller's output serves as Ibat. The specified outer loop expressions are:

$$I_{bat}^*(k) = I_{bat}^*(k-1) + k_{pV}\{V_{bate}(k) - V_{bate}(k-1)\} + k_{iV} \cdot V_{bate}(k)$$

where kpV stands for the proportional gain of the voltage PI controller, kiV for the integral gain, and k

for the sampling moment. Inner loop control is implemented by comparing the current used to charge Ibat to Ibat, and sending the error (Ie) to the control circuit after that.The needed duty ratio (mc) is provided by the PI controller's output as

$$m_c^*(k) = m_c^*(k-1) + k_{pI}\{I_e(k) - I_e(k-1)\} + k_{iI} \cdot I_e(k)$$

where kpI and kiI, respectively, are the gains of the current PI controller. Next, the duty ratio (mc) is compared to a carrier waveform. Switch (S1 and S2) receive the relevant gate drive signals from the comparison.

2.4 Speed Control Strategy

The DC reference voltage (V^*_{dc}) is provided below is calculated with the help of reference speed.

$$V^*_{dc} = k_v \omega^*$$

The reference voltage (V^*_{dc}) is compared with the actual load voltage (V_{dc}) and the error voltage (V_E) is provided below as

$$V_E = V^*_{dc} - V_{dc}$$

The generated error is given to proportional–integral (PI) control, which provides the reference voltage V_C as follows:

$$V_C(k) = V_C(k-1) + K_P \{V_E(k) - V_E(k-1)\} + K_i V_E(k)$$

The pulses generated for the boost converter is as follows:

{If $M_C < V_C$ gating pulse is HIGH}

{If $M_C \geq V_C$ gating pulse is LOW}

3 SIMULATION SETUP & RESULTS

The simulation parameters for the proposed converter are shown below in Table I:

Input Voltage	(160 -230) V
Input power	1500W
Switching Frequency	2 KHZ
Inductor	9.1mH
Coupling Capacitor	55.6µF
Output Capacitor	2mF
Battery voltage	48V
Battery capacity	1.5Ah

DC Motor parameters	150V, 500W, 1500 rpm

The simulation circuit for the cuk converter with PI controller is provided below in fig.10.

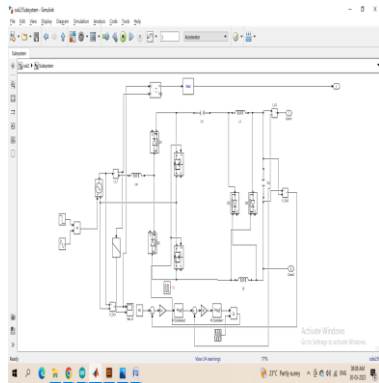Figure 10: Simulation circuit.

In this, the supply voltage of 230V is applied to the proposed converter from t=0 to t=0.3s. Then the supply changed from 230V to 160V at t=0.3s. During this two modes, the battery will be charging and the motor will be in standstill condition. The simulation circuit for the high gain bidirectional converter with PI controller is provided below:
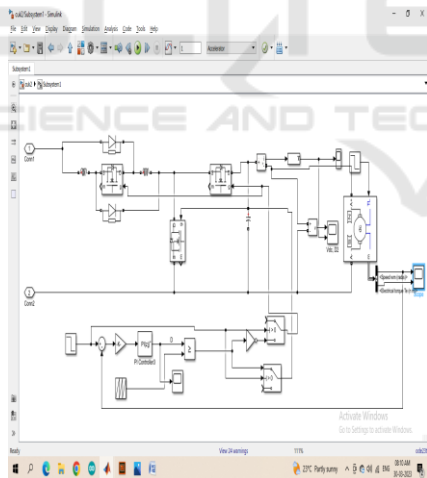

Figure 11: Bii-directional converter simulation.

The motor begins to function in the forward direction and the battery begins to discharge at t=0.6s (mode 3). Regenerative braking is performed to the motor at t=0.95s (mode 4), and the charge stored in the motor windings is extracted to recharge the battery.

In mode1 and 2, the supply is connected and charges the battery of the EV. The supply voltage and current is provided is provided below:
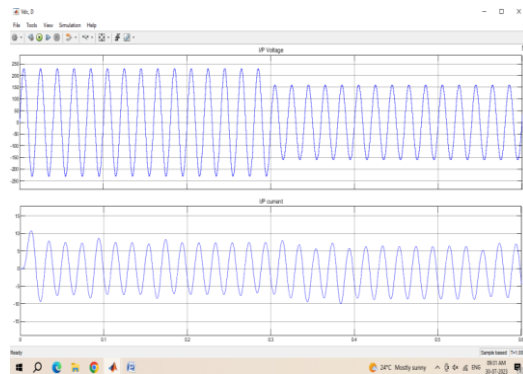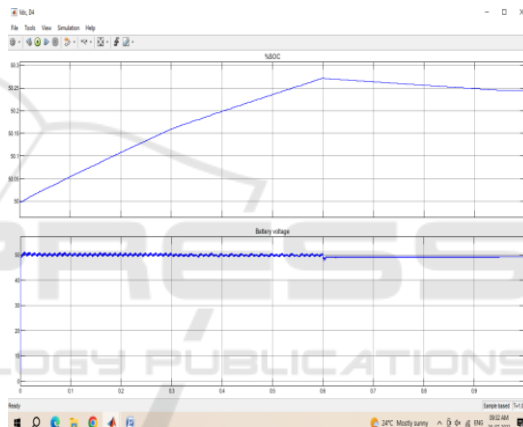

Figure 12: Supply voltage and current.

The supply voltage in this is around 220V and 7A. The supply charges the battery, and the waveforms of its voltage and%SOC are shown below voltage), and the SOC:

This keeps the battery voltage at 52V (which is greater than the 48V battery nominal percentage is rising. At t=0.6s, the supply is cut off, and as the battery begins to discharge and deliver power to the car, the%SOC starts to fall. Below are the motor voltage and current values:
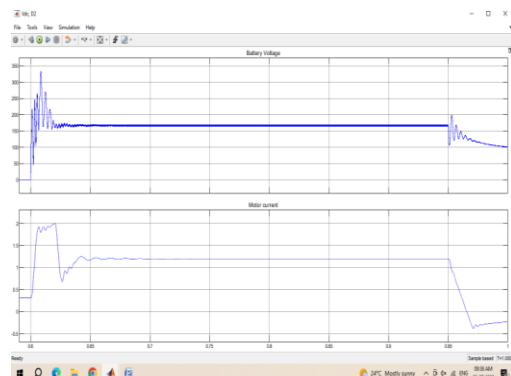

Figure 13: Motor voltage and current.

At t=0.6s, the motor begins to run in the forward direction with a positive current flow, and at t=0.95s, regenerative braking is performed with a negative current flow, or it is supplied back to the battery to charge it. Below is a list of the battery voltage and SOC during regenerative braking:
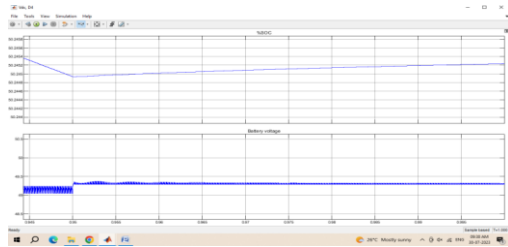

Figure 14: battery voltage and SOC.

The battery is first charged by the source until t=0.6s, resulting in a high battery voltage and rising SOC. The soc starts to decrease as the engine turns on at time t=0.6s as a result of battery discharge. Regenerative braking is used at time 0.95 seconds, which recharges the battery once more and raises the voltage and %SOC.The %THD of the supply current is provided below:
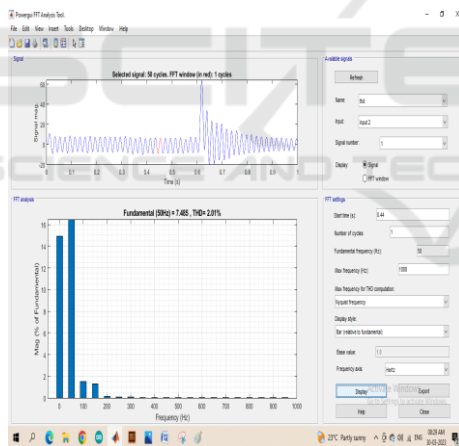

Figure 15: Total Hamonic Distortion.

The %THD of the supply current is around 2.01%. The efficiency of the proposed system is provided below: With an efficiency of about 95%, the input power is in the range of 1570W and the output power is about 1500W.
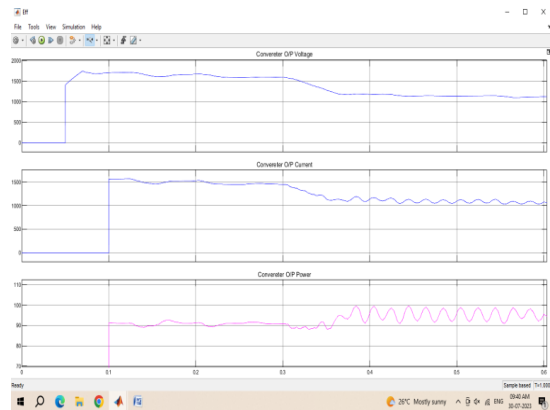

Figure 16: Simulation results.

Using a battery of 12V, 2.2Ah and a BSIC converter with an output voltage of 24V, 50 Hz, a hardware prototype model of the proposed converter is created. When the battery is being discharged, the input voltage of the battery is 12V, and the load voltage of the high gain converter is 48V. The hardware specifications are listed in Table II below.

Table 2: Hardware Parameters.

IRF 250N - MOSFET	200v, 30A
U1560-DIODE	200-400-600v, 15a
Capacitor	1000μF, 25V
	1000μF, 100V
TRANSFORMER	12V, 1A
TLP 250 – DRIVER IC	12V, 1.5A
CD 4050 BUFFER IC	3-18V, 0.32mA
12V REGULATOR 7812	12V, 1A
IN 4007 DIODE	700V, 1A
ARDUINO UNO CONTROLLER	7-12V, 20mA

The suggested converter uses an Arduino uno control to generate the pulses, which are then sent to the driver circuit (TLP 250) to drive the mosfets IRF 250. Below are the input voltage waveforms:
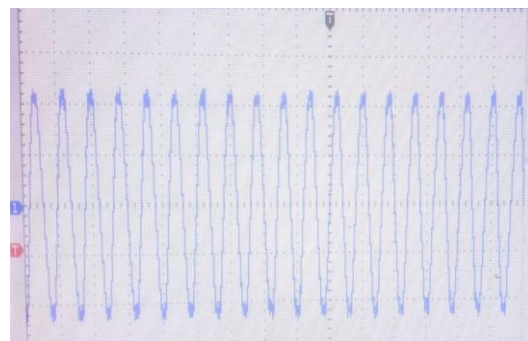

Figure 17: Voltage.

In this the voltage division is 10V/div and the input voltage is around 24V. It is provided to charge the battery. The battery voltage is provided below:
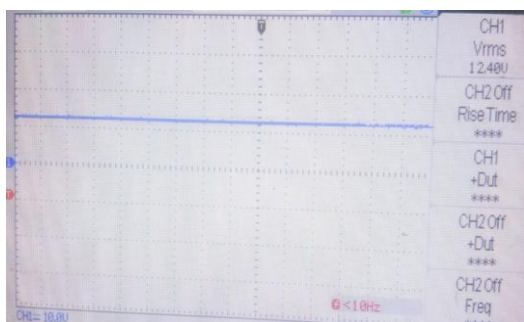

Figure 18: Battery charging and Discharging.

In battery discharging mode, the battery voltage is provided as input and the load voltage is provided below:

Figure 19: Load voltage.

The load voltage of the high gain converter is around 40.4V.

Fig 20: Prototype model of proposed converter.

4 CONCLUSION

The size of the converter is decreased as the bridge is removed from the switched inductor (SI) based Cuk converter that was designed in this research for use with electric vehicles. A high gain bidirectional converter is introduced to power the motor for the operation of an electric vehicle after the performance of the converter under steady state and transient situations is noted. Regenerative braking is used to extend the vehicle's range by restoring energy from the motor to the battery. The simulation results show that the proposed converter is 95% efficient. A hardware prototype model was created, and the suggested system's functionality was checked.

REFERENCES

Lachvajderova, Laura & Kadarova, Jaroslava. (2021)Analysis Of Internal Combustion Engine Vehicle, Battery Electric Vehicle And Emissions From Transport. 21. 21-33.

Wang, L., Qin, Z., Slangen, T., Bauer, P., & van Wijk, T. (2021). Grid Impact of Electric Vehicle Fast Charging Stations: Trends, Standards, Issues and Mitigation Measures - An Overview. *IEEE Open Journal of Power Electronics*, *2*, 56–74. https://doi.org/10.1109/ojpel.2021.3054601

Bahrami, Ali. (2020). EV Charging Definitions, Modes, Levels, Communication Protocols and Applied Standards. 10.13140/RG.2.2.15844.53123/11

Dulau, Lucian Ioan & Bica, Dorin. (2020). Effects of Electric Vehicles on Power Networks. Procedia Manufacturing. 46. 370-377. 10.1016/j.promfg.2020.03.054.

Khalid, Mohd & Khan, Irfan & Hameed, Salman & Asghar, M. & Ro, Jong-Suk. (2021). A Comprehensive Review on Structural Topologies, Power Levels, Energy Storage Systems, and Standards for Electric Vehicle Charging Stations and Their Impacts on Grid. IEEE Access. PP. 1-1. 10.1109/ACCESS.2021.3112189.

Das, Manoj & Jain, Sachin. (2021). Review on Optimization Techniques used for Scheduling of Electric Vehicle Charging. 1-6. 10.1109/CAPS52117.2021.9730621.

Rachid, A., El Fadil, H., Gaouzi, K., Rachid, K., Lassioui, A., El Idrissi, Z., & Koundi, M. (2022). Electric Vehicle Charging Systems: Comprehensive Review. *Energies*, *16*(1), 255. https://doi.org/10.3390/en16010255

Habib, S., Khan, M. M., Abbas, F., Sang, L., Shahid, M. U., & Tang, H. (2018). A Comprehensive Study of Implemented International Standards, Technical Challenges, Impacts and Prospects for Electric Vehicles. *IEEE Access*, *6*, 13866–13890. https://doi.org/10.1109/access.2018.2812303

Sanguesa, J. A., Torres-Sanz, V., Garrido, P., Martinez, F. J., & Marquez-Barja, J. M. (2021). A Review on Electric Vehicles: Technologies and Challenges. *Smart Cities*, *4*(1), 372–404. MDPI. https://doi.org/10.3390/smartcities4010022

Sanguesa, J. A., Torres-Sanz, V., Garrido, P., Martinez, F. J., & Marquez-Barja, J. M. (2021). A Review on Electric Vehicles: Technologies and Challenges. *Smart Cities*, *4*(1), 372–404. MDPI. https://doi.org/10.3390/smartcities4010022